Journal of Sound and Vibration (1999) **222**(5), 699–722
Article No. jsvi.1998.2127, available online at http://www.idealibrary.com on IDEAL®

A THIRD-ORDER BOUNDARY ELEMENT METHOD FOR EXTERIOR ACOUSTICS WITH APPLICATIONS TO SCATTERING BY RIGID AND ELASTIC SHELLS

M. GENNARETTI, A. GIORDANI AND L. MORINO
Dipartimento di Ingegneria Meccanica e Industriale, University of Rome III, via della Vasca Navale 79, 00146 *Rome, Italy*

(*Received* 12 *February* 1998, *and in final form* 19 *October* 1998)

In this work a novel third-order direct boundary element method for the Helmholtz equation is presented. The methodology is best understood within the context of the so-called "fictitious eigenvalues difficulty", introduced by the typical direct boundary integral approach; this problem consists of the existence of fictitious resonance frequencies (i.e., frequencies of the adjoint interior problem) and is overcome by the CONDOR technique by Burton and Miller (i.e., a suitable linear combination of the Kirchhoff–Helmholtz integral equation with that obtained by taking its normal derivative). This in turn yields the presence of a hypersingular kernel (arising in the integral expression for the normal derivative of the Kirchhoff–Helmholtz integral equation), which is regularized by introducing a novel integral relationship (closely related to the equivalence between doublet layers and vortex layers in incompressible potential flows). This requires the evaluation of the tangential Laplacian of the unknown, and hence the use of a high-order discretization. A piecewise bicubic discretization of the boundary integral equation is used in this paper. The resulting equation contains only the nodal values of the unknown. Numerical applications to particularly taxing problems (such as high-frequency radiation and scattering problems of rigid and elastic shells) are included, and validated through comparison with analytical solutions. Numerical results show that the convergence rate is of order h^3 (h being the typical element size), even for high-frequency analysis, indicating that this is a true third-order method.

1. INTRODUCTION

This paper presents a third-order boundary element methodology for the analysis of exterior acoustics. Applications include particularly taxing problems, such as scattering of rigid shells, as well as vibration and scattering of elastic shells, for a frequency range (up to $ka = 30$) which is unusually high for boundary element methods.

The pressure field, governed by the Helmholtz equation, is here determined by a boundary-element solution of the Kirchhoff–Kelmholtz boundary integral

0022–460X/99/200699 + 24 $30.00/0

equation. A drawback in using a boundary integral method in this type of analysis arises from the so-called "fictitious eigenvalue difficulty", since the Kirchhoff–Helmholtz boundary integral equation is affected by spurious (characteristic) frequencies (solution is not unique at those frequencies). These correspond to the adjoint interior problem eigenvalues (see reference [1]); indeed, when using a Neumann exterior integral operator of the second kind, the resonant frequencies of the corresponding Dirichlet interior problem (first kind) would appear in its spectrum, whereas in the spectrum of the exterior Neumann integral operator of the first kind, the resonant frequencies of the corresponding Neumann interior problem would appear. This fictitious eigenvalue difficulty is one of the primary issues in the current research on boundary integral equations as applied to acoustics (this non-physical resonances can completely destroy the solution of the numerical method used to solve the Kirchhoff–Helmholtz equation).

A review of the most significant work in the field of acoustic wave scattering is beyond the scope of the present paper. An excellent introduction to the field is the book by Colton and Kress [1]. Some of the work closely related to the argument of the present paper include that of Schenck [2], Jones [3], Ursell [4], and Amini [5], where the regularization of the boundary integral equation for the exterior Helmholtz problem is examined, that of Amini and Kirkup [6], where the behavior of elementary boundary integral equations and of their discrete boundary element counterparts close to spurious frequencies is studied, and that of Gallman *et al*. [7], where the scattering of rigid bodies is analyzed by different frequency-domain boundary integral approaches. Extensive reviews on the problem of acoustic wave scattering, including the issue of regularization of the boundary integral equation, have been written by Gaunaurd [8], Amini and Harris [9], and Amini *et al*. [10].

In this work, we adopt a classical method of regularization for the integral equation, known as CONDOR (Composite Outward Normal Derivative Overlap Relation) technique, suggested by Burton and Miller [11]. This consists of solving a suitable linear combination of the Kirchhoff–Helmholtz equation for the unknown function with that obtained by taking its normal derivative. In fact, although the Kirchhoff–Helmholtz integral operator and the integral equation for the normal derivative are both affected by the spurious resonances at the characteristic frequencies of the cavity (for the Dirichlet and Neumann problem, respectively), it was proved that the combination of the two equations circumvents this problem (see references, [1, 11]). This formulation gives rise to a hypersingular kernel in the resulting boundary integral equation. The problem of solving the hypersingular integral equation in three-dimensional external acoustics has been investigated by several authors; among them, Meyer *et al*. [12] circumvent the hypersingularity by considering tangential operators (constant values of variables over flat elements of discretization are required in this technique), Terai [13] introduces a closed-form evaluation of the hypersingular integral, under the assumption of flat triangular elements of discretization, whereas Chien *et al*. [14] obtain the regularization by employing some identities arising in the integral equation for the Laplace equation in the interior domain.

Here, the problem is circumvented by applying a regularization technique based on the integral equivalence discussed in Appendix A. This requires the evaluation of the tangential Laplacian of the unknown. Thus, the discretization of the resulting integral equation is performed by using a high-order algorithm introduced in references [15, 16] for the potential problem, which consists of a bicubic distribution over each boundary element for all the variables involved in the problem under consideration, i.e., geometry, velocity potential, φ, and normal derivative, $\partial\varphi/\partial n$. Such an algorithm has the following characteristics: (1) it yields a smooth solution; (2) it requires a topological structure for the discretization that (in contrast with typical high-order schemes) is user friendly (specifically, as simple as a first-order discretization); (3) the unknown is described in terms of a limited number of parameters (specifically, only the nodal values of the unknown and not its tangential derivatives); (4) the scheme has a high rate of convergence (quite useful, in particular, for high-frequency problems; indeed, the convergence rate is of the order of h^3, as for a true third-order numerical algorithm).

The boundary integral approach used here, including the regularization technique, is presented in section 2. Section 3 describes the third-order numerical algorithm used for the discretization of the boundary integral equation. Numerical results concerning scattering of rigid and elastic shells are presented in section 4, where thay are compared with analytical results. Appendices A and B discuss the regularization of the hypersingular kernel arising from the application of the CONDOR technique. Appendix C examines the order of convergence.

2. EXTERIOR ACOUSTICS

This section addresses the analysis of the exterior pressure field for a body, immersed in an unbounded medium, that is vibrating and/or is impinged by an acoustic wave of given frequency and amplitude.

First, note that in the frequency-domain, using linearized Bernoulli's theorem, the perturbation pressure field, p', can be expressed in terms of velocity potential, φ, as

$$p' = p - p_0 = -\mathrm{i}\omega\rho_0\varphi, \tag{1}$$

where $\mathrm{i} = \sqrt{-1}$, ω is the angular frequency of the acoustic wave, and p_0 and ρ_0 are the pressure and the density of the undisturbed medium, respectively (note that equation (1) is obtained setting $\hat{p}'(\mathbf{x}, t) = p'(\mathbf{x})\exp(\mathrm{i}\omega t)$ and $\hat{\varphi}(\mathbf{x}, t) = \varphi(\mathbf{x})\exp(\mathrm{i}\omega t)$. Assuming the flow to be isentropic and combining the linearized continuity equation with the linearized Bernoulli theorem, one obtains the Helmholtz equation,

$$\nabla^2\varphi + k^2\varphi = 0, \tag{2}$$

where $k = \omega/c$ is the wave number, with c denoting the speed of sound of the undisturbed medium. Let

$$\varphi = \varphi^I + \varphi^S, \tag{3}$$

where φ^I and φ^S denote, respectively, the incident and the scattered potential. Since the incident-potential wave satisfies equation (2), this is true for φ^S as well. The boundary integral representation for the scattered velocity potential is (see, e.g., reference [1])

$$\varphi^S(\mathbf{x}) = \int_{\mathcal{S}} \left[\frac{\partial \varphi^S}{\partial n} G - \varphi^S \frac{\partial G}{\partial n} \right] \mathrm{d}\mathcal{S}(\mathbf{y}), \tag{4}$$

where $G = -\exp(-\mathrm{i}kr)/4\pi r$ is the fundamental solution of the Helmholtz equation, with $r = \| \mathbf{y} - \mathbf{x} \|$, and $\mathcal{S}$ denotes the body surface.

The Neumann boundary condition on $\mathcal{S}$ is given by $\partial\varphi/\partial n = \mathrm{i}\omega w$, where w denotes the normal displacement of the shell surface (preservation of continuity on S between surface velocity and normal fluid velocity); therefore,

$$\frac{\partial \varphi^S}{\partial n} = -\frac{\partial \varphi^I}{\partial n} + \mathrm{i}\omega w. \tag{5}$$

Coupling this condition with the boundary integral representation in equation (4), one obtains an exterior Neumann integral operator of the second kind which, as stated in section 1, is non-uniquely solvable at the eigenvalues of the corresponding interior Dirichlet problem [1]. Here, in order to avoid the occurrence of fictitious resonant frequencies in the problem mentioned above, the CONDOR approach by Burton and Miller [11] is used, in which the regularization is obtained by combining equation (4) with the integral representation of its derivative with respect to the normal of surface at the observation point, $\mathbf{x}$, for $\mathbf{x} \in \mathcal{S}$, i.e.,

$$\frac{\partial \varphi^S}{\partial n}(\mathbf{x}) = \lim_{\mathbf{x}' \to \mathbf{x}} \mathbf{n}_x(\mathbf{x}) \cdot \int_{\mathcal{S}} \left[\frac{\partial \varphi^S}{\partial n} \nabla' G(\mathbf{x}', \mathbf{y}) - \varphi^S \nabla' \frac{\partial G}{\partial n}(\mathbf{x}', \mathbf{y}) \right] \mathrm{d}\mathcal{S}(\mathbf{y}), \tag{6}$$

where $\mathbf{n}_x(\mathbf{x})$ is the unit vector normal to the surface $\mathcal{S}$ at the point $\mathbf{x} \in \mathcal{S}$, and ∇' denotes the gradient with respect to the variable $\mathbf{x}'$. Note that, the kernel in the second term in equation (6) is hypersingular: the evaluation of such contribution is discussed in Appendix A. Hence, applying the CONDOR approach, the distribution on the body surface of the scattered velocity potential is obtained from the following linear combination of equations (4) and (6):

$$\begin{aligned} \varphi^S(\mathbf{x}) + \eta \frac{\partial \varphi^S}{\partial n}(\mathbf{x}) = & \lim_{\mathbf{x}' \to \mathbf{x}} \int_{\mathcal{S}} \left[\frac{\partial \varphi^S}{\partial n} G(\mathbf{x}', \mathbf{y}) - \varphi^S \frac{\partial G}{\partial n}(\mathbf{x}', \mathbf{y}) \right] \mathrm{d}\mathcal{S}(\mathbf{y}) \\ & + \eta \lim_{\mathbf{x}' \to \mathbf{x}} \mathbf{n}_x(\mathbf{x}) \cdot \int_{\mathcal{S}} \left[\frac{\partial \varphi^S}{\partial n} \nabla' G(\mathbf{x}', \mathbf{y}) - \varphi^S \nabla' \frac{\partial G}{\partial n}(\mathbf{x}', \mathbf{y}) \right] \mathrm{d}\mathcal{S}(\mathbf{y}), \end{aligned} \tag{7}$$

where $\eta = \eta(k)$ is a function of the wave number. It has been shown that, in case of scattering by bodies with regular surfaces, a good choice for the coefficient of

the linear combination in equation (7) is $\eta = i2$ for $k \leqslant 1/2$ [9], whereas for $k > 1/2$ a good choice is $\eta = i(1/k)$ [5, 17]; these values have been used for all the results presented in this work.

3. THIRD-ORDER FORMULATION

This section, discusses the third-order numerical algorithm and then applies it to the specific problem under consideration.

For the sake of clarity, consider first a two-dimensional problem. If $u(\mathbf{x})$ represents a variable of interest, and $\xi \in [-1, 1]$ is the domain of integration for each boundary element, one may use the Hermite polynomials,

$$h_{1,2}(\xi) = \frac{1}{4}(2 \mp 3\xi \pm \xi^3) \quad \text{and} \quad h_{3,4}(\xi) = \frac{1}{4}(\pm 1 - \xi \mp \xi^2 + \xi^3),$$

in order to obtain the following cubic interpolation formula

$$\check{u}(\xi) = u^- h_1(\xi) + u^+ h_2(\xi) + u_\xi^- h_3(\xi) + u_\xi^+ h_4(\xi),$$

where $u^\pm$ represents values of function u in $\xi = \pm 1$, and $u_\xi^\pm$ represents values of ξ-derivative of u in $\xi = \pm 1$ (i.e., an interpolation of class $C^{1,\alpha}$).

In the three-dimensional case, the surface is divided into quadrilateral elements. The subdivision into elements is such that the nodes on the edge of one element coincide with those on the edge of the adjacent element. For each element, a local co-ordinate system $(\xi, \eta) \in [-1, 1] \times [-1, 1]$ is defined, and the interpolation is obtained by combining Hermite's interpolation along each co-ordinate line. Specifically, on each element, one has the following interpolation

$$\check{u}(\xi, \eta) = \sum_{j=1}^{16} \hat{u}_j f_j(\xi, \eta), \tag{8}$$

where

$$\mathbf{f}(\xi, \eta) = \begin{Bmatrix} f_1(\xi, \eta) \\ f_2(\xi, \eta) \\ \cdots \\ f_{16}(\xi, \eta) \end{Bmatrix} = \begin{Bmatrix} h_2(\xi)h_2(\eta) \\ h_2(\xi)h_1(\eta) \\ \cdots \\ h_3(\xi)h_3(\eta) \end{Bmatrix}$$

and

$$\hat{\mathbf{u}} = \begin{Bmatrix} \hat{u}_1 \\ \hat{u}_2 \\ \cdots \\ \hat{u}_{16} \end{Bmatrix} = \begin{Bmatrix} u^{++} \\ u^{+-} \\ \cdots \\ u_{\xi\eta}^{--} \end{Bmatrix},$$

where the $\hat{u}_j$ $(j = 1, 16)$ are the values of function u, of its ξ-derivative, of its η-derivative and of its $\xi\eta$-second derivative, at the four corners of the element; specifically,

$$u^{++} = u(1, 1), \quad u^{+-} = u(1, -1), \quad u^{-+} = u(-1, 1), \quad u^{--} = u(-1, -1),$$
$$u_\xi^{++} = u_\xi(1, 1), \quad u_\xi^{+-} = u_\xi(1, -1), \quad u_\xi^{-+} = u_\xi(-1, 1), \quad u_\xi^{--} = u_\xi(-1, -1),$$
$$u_\eta^{++} = u_\eta(1, 1), \quad u_\eta^{+-} = u_\eta(1, -1), \quad u_\eta^{-+} = u_\eta(-1, 1), \quad u_\eta^{--} = u_\eta(-1, -1),$$
$$u_{\xi\eta}^{++} = u_{\xi\eta}(1, 1), \quad u_{\xi\eta}^{+-} = u_{\xi\eta}(1, -1), \quad u_{\xi\eta}^{-+} = u_{\xi\eta}(-1, 1), \quad u_{\xi\eta}^{--} = u_{\xi\eta}(-1, -1).$$

Note that this assures that the function is continuous over the whole boundary surface and that its first derivatives are continuous at the nodes of the panel.* Next, note that (key to the method) one wants to express the nodal values of the derivatives of u in terms of the nodal values of u. Consider first the first-order derivatives, u_ξ and u_η. Note that these depend upon the co-ordinate system (i.e., for a given node, the values of u_ξ and u_η depend upon the co-ordinate system of the element under consideration). Note, however, that u_ξ and u_η are the covariant components of $\nabla_t u$ (tangent gradient of u), and that $\nabla_t u$ is independent of the co-ordinate system (i.e., for a given node, $\nabla_t u$ is independent of the element; for instance, for $u = \varphi$, $\nabla_t \varphi$ is the tangential portion of the velocity vector). Thus, in order to obtain user friendliness (see below), the tangent gradient is calculated at each node as the average over those on all the elements that have the node as a corner. The derivatives within each element are evaluated by appropriate non-centered (first-order) finite difference using the values of the function at the corners of the same element.† Thereafter, u_ξ and u_η for an element at the node under consideration are obtained by dotting $\nabla_t u$ with the appropriate covariant base vector of that element. Next, consider the $u_{\xi\eta}$ derivative. This is assumed to have a constant value on each element, and equal to that evaluated by finite differences at the center of the element (obtained from the values of the function at the corners of it).

As mentioned above, the resulting scheme is user friendly. Indeed, the procedure outlined above allows one to use a very simple topological structure for the description of the geometry. For, each panel is treated independently of the others. Thus, the procedure is applicable also to those nodes where there exists a discontinuity in the local co-ordinate directions, e.g., nodes on the plane of symmetry of a swept wing (and in general, on the boundaries of the patches in which the boundary surface is usually subdivided). The only information required is the topological function that gives the global nodal number in terms of the global element number and the number of the corner of the panel (which the authors have used in the past for a first-order discretization of the geometry).‡

*This is not necessarily true at the edge points, because $u_{\xi\eta}$ depends upon the element co-ordinates; however, if (ξ, η) denotes a co-ordinate system that is continuous over a whole patch (collection of elements), then the interpolation $\breve{u}$ will be of class $\mathcal{C}^{1,\alpha}$ over the whole patch.

†Note that although the approximations of the derivatives are of first order, as shown later, the resulting overall scheme is still of third order.

‡Note, however, that for all the results presented here, the base vectors, $\partial\mathbf{x}/\partial\xi$ and $\partial\mathbf{x}/\partial\eta$, are evaluated analytically (and not by finite differences).

Using the above mentioned procedure to relate the various derivatives to the nodal values of u, one obtains a matrix $\mathbf{T}$ such that $\hat{\mathbf{u}}^{\mathrm{T}} = \mathbf{u}^{\mathrm{T}}\mathbf{T}$, where $\hat{\mathbf{u}}$ are the parameters in equation (8), whereas $\mathbf{u}$ is the global vector of the nodal values of u. Hence, the numerical algorithm described yields the following interpolation for u on each boundary element

$$\breve{u}(\xi, \eta) = \mathbf{u}^{\mathrm{T}}\mathbf{T}\mathbf{f}(\xi, \eta). \tag{9}$$

Finally, observe that equation (9) may be rewritten as

$$\breve{u}(\mathbf{x}) = \mathbf{u}^{\mathrm{T}}\mathbf{g}(\mathbf{x}) = \sum_{j=1}^{N_N} u_j g_j(\mathbf{x}), \tag{10}$$

(where N_N is the number of nodes) with

$$\mathbf{g}(\mathbf{x}(\xi, \eta)) := \mathbf{T}\mathbf{f}(\xi, \eta), \tag{11}$$

where $\mathbf{g}(\mathbf{x})$ is the vector of the N_N global shape functions (defined piecewise), which are such that $g_j(\mathbf{x}_i) = \delta_{ji}$ (with δ_{ji} denoting the Kronecker delta).

By construction, the global functions $g_j(\mathbf{x})$ are continuous over the surface of the boundary. Their first derivatives are continuous in the interior of the elements and at the nodes. They are not continuous at the edge points because $u_{\xi\eta}$ at a given node assumes a different value for each element connected with that node. Nonetheless, the numerical results indicate that the resulting scheme behaves like a true third order scheme (even if, as mentioned above, a first-order finite difference has been used for the derivatives).

3.1. DISCRETIZATION OF INTEGRAL EQUATION

Combining equations (7) and (10), and using the collocation method, one obtains the discretized expression of the integral equation for the scattered potential

$$\frac{1}{2}[\varphi_k^S + \eta\chi_k^S] = \sum_{j=1}^{N_B}(B_{kj}\,\chi_j^S + C_{kj}\,\varphi_j^S) + \eta\sum_{j=1}^{N_B}(\hat{B}_{kj}\,\chi_j^S + \hat{C}_{kj}\,\varphi_j^S), \tag{12}$$

where N_B is the number of nodes on the body surface, whereas $\chi^S = \partial\varphi^S/\partial n$ is known from the boundary conditions, equation (5). The coefficients of equation (12) are given by

$$B_{kj} = \int_{\mathcal{S}_B} G(\mathbf{x}_k, \mathbf{y})g_j(\mathbf{y})\,\mathrm{d}\mathcal{S}(\mathbf{y}), \quad C_{kj} = \int_{\mathcal{S}_B} \frac{\partial G}{\partial n}(\mathbf{x}_k, \mathbf{y})g_j(\mathbf{y})\,\mathrm{d}\mathcal{S}(\mathbf{y}), \tag{13}$$

$$\hat{B}_{kj} = \int_{\mathcal{S}_B} \frac{\partial G}{\partial n_k}(\mathbf{x}_k, \mathbf{y})g_j(\mathbf{y})\,\mathrm{d}\mathcal{S}(\mathbf{y}), \quad \hat{C}_{kj} = \int_{\mathcal{S}_B} \frac{\partial^2 G}{\partial n_k \partial n}(\mathbf{x}_k, \mathbf{y})g_j(\mathbf{y})\,\mathrm{d}\mathcal{S}(\mathbf{y}), \tag{14}$$

where g_j are those of equation (10), whereas $G_k = -\exp(-\mathrm{i}kr_k)/4\pi r_k$, with $r_k = \| \mathbf{y} - \mathbf{x}_k \|$, where $\mathbf{x}_k$ are the collocation points. Furthermore, $\partial/\partial n_k$ denotes differentiation along the direction normal to the body surface at the kth

collocation point. Note that the discretization used implies that the points of the boundary surface are smooth. Note also that integrals in equations (13) and (14) are weakly singular, except for the hypersingular integral $\hat{C}_{kj}$; however, $\hat{C}_{kj}$ may be expressed as the sum of weakly singular integrals after the application of regularization technique described in Appendix A. For the numerical application of the formulation, weakly singular integrals have been transformed into regular ones by considering polar co-ordinates, and then the Gauss–Legendre quadrature formula has been used to evaluate them (see, e.g., references [16, 18]).

4. NUMERICAL RESULTS

In this section, results obtained with the formulation presented above are presented. First, the capability of the formulation to overcome the fictitious eigenvalue difficulty is shown; then, the sound scattered by a rigid sphere impinged by a planar wave is analyzed; finally, the same problem is studied by assuming the sphere to be an elastic shell; the results are validated through comparisons with analytical solutions. Details about analytical solutions for the problems examined in sections 4.1 and 4.2 are given in reference [19], whereas the analytical solution for sound scattered by elastic shells is given in reference [20].

4.1. FICTITIOUS EIGENVALUE DIFFICULTY

In order to discuss the issues related to the fictitious eigenvalue difficulty, consider a sphere of radius a, with a radially pulsating surface (Neumann problem of the second kind for the Helmholtz equation). Figures 1 and 2 depict amplitude and phase angle of the (spatially constant) potential on the surface of

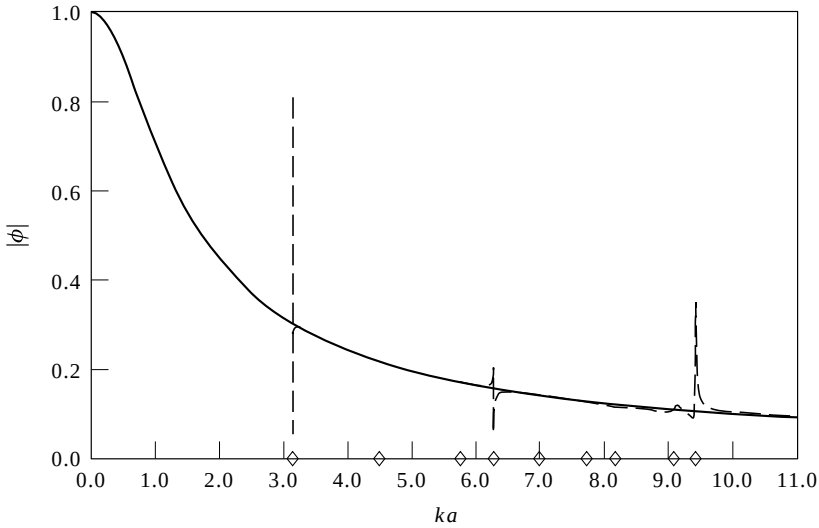

Figure 1. Amplitude of potential on the surface of a pulsating sphere as a function of the pulsation wave number. ——, Analytical solution; – – –, BEM equation (4) with $N = 4$; ◇, spurious frequencies.

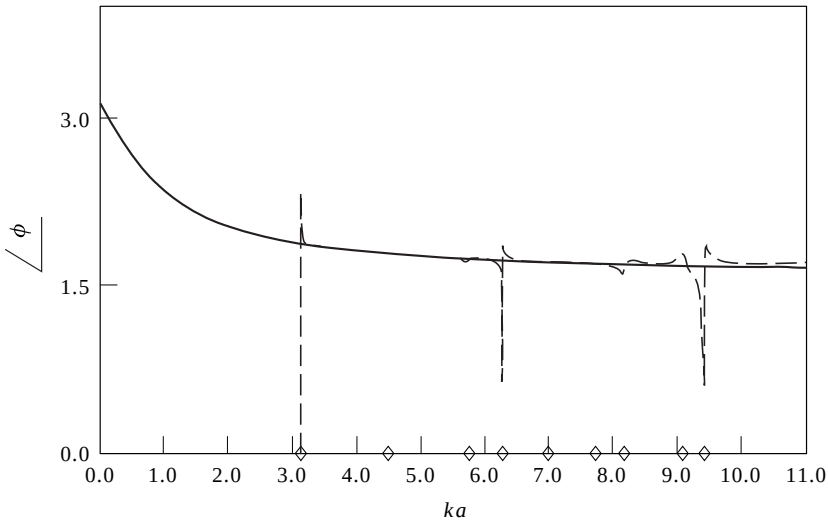

Figure 2. Phase angle of potential on the surface of a pulsating sphere as a function of the pulsation wave number. ——, Analytical solution; – – –, BEM equation (4) with $N = 4$; ◇, spurious frequencies.

the sphere, as a function of the pulsation wave number, k (a unit-amplitude potential normal derivative, χ, has been considered). Specifically, the analytical solution of potential on the body surface is compared with the numerical solution obtained from equation (4) (usual BEM approach), showing a good agreement except when k is equal to the spurious frequency values (eigenvalues of internal Dirichlet problem for the sphere, obtained as zeroes of the spherical Bessel functions [1]). The numerical solution is indeed regularized by the CONDOR approach of Burton and Miller [11], as demonstrated in Figures 3 and 4, where it is shown that the numerical solution obtained from equation (7) (regularized BEM approach, referred to as "present formulation" in all of the captions of this work), is in good agreement with the analytical solution, even at spurious frequency values (the numerical solution has been evaluated for $N = 4$, with N representing the number of elements along the meridians of the spherical surface, and half of the number of elements along the parallels; see Figure 5 for an illustration of the type of boundary element mesh used in this work).

The behavior of the numerical solution as a function of the number of boundary elements is examined in Appendix C, and shows a third-order rate of convergence to the analytical solution.

4.2. SCATTERING BY A RIGID SPHERE

First, consider a near-field potential scattered by a sphere of radius a. For a unit-amplitude impinging plane wave with wave number, k, such that $ka = 1$, Figure 6 depicts the comparison between the analytical solution and the present numerical results in terms of the variation of scattered potential as a function of the polar angle, at a distance $d = 5a$ from the center of the sphere (this result has been obtained using $N = 48$, and hence the distance between the parallels of discretization equals $\Delta s = \lambda ka/2N = \lambda/96$, with λ denoting the wavelength). The

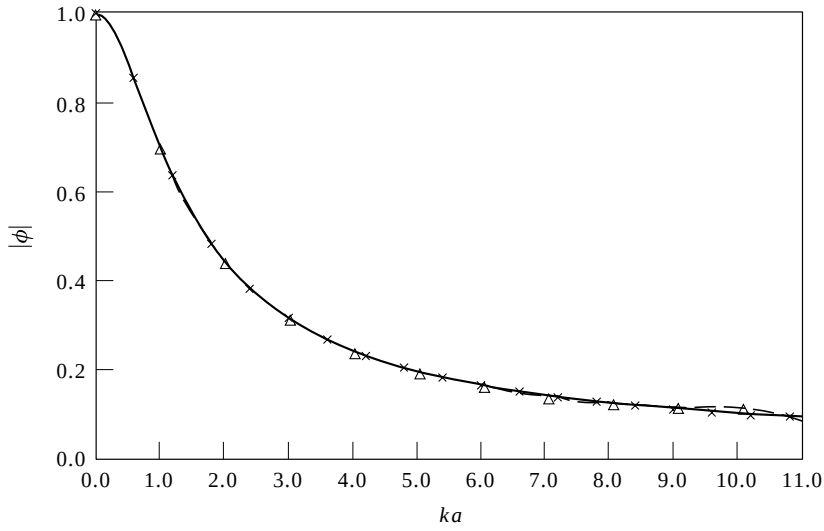

Figure 3. Amplitude of potential on the surface of a pulsating sphere as a function of the pulsation wave number. ——, Analytical solution; △——△, present formulation with $N = 3$; ×----×, present formulation with $N = 4$.

numerical results shown are both those obtained by solving equation (4), and those obtained by the regularized integral formulation given by equation (7). In this case, these numerical results are identical since the frequency of the impinging wave is not a spurious frequency for the sphere. Very different results are obtained when the case of a unit-amplitude impinging plane wave with $ka = \pi$ is considered. Indeed, $ka = \pi$ is the first spurious frequency of the sphere

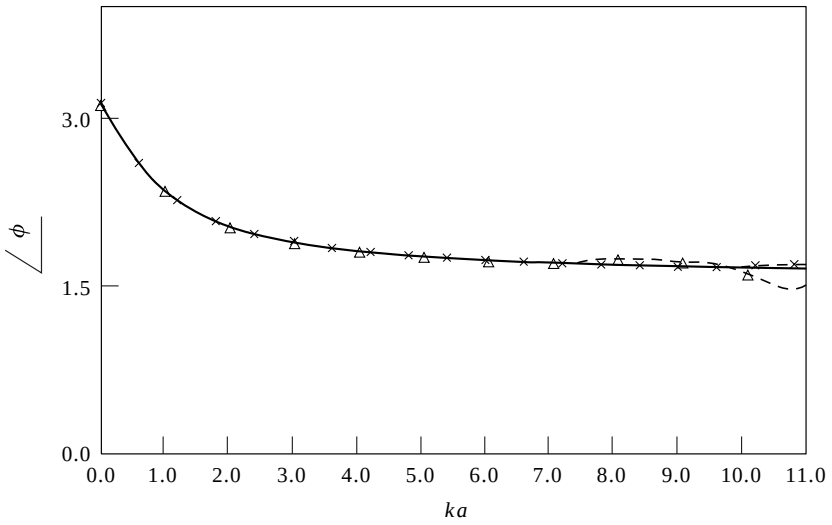

Figure 4. Phase angle of potential on the surface of a pulsating sphere as a function of the pulsation wave number. ——, Analytical solution; △——△, present formulation with $N = 3$; ×----×, present formulation with $N = 4$.

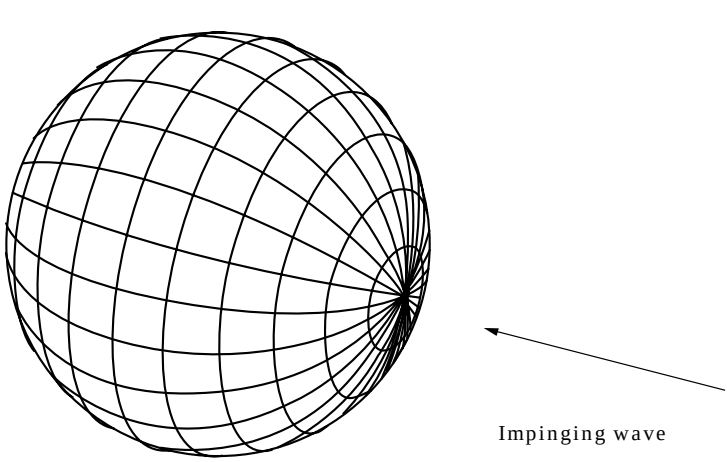

Figure 5. Discretization of the sphere with $N = 12$.

and, as shown in Figure 7, the numerical result from the usual BEM approach (equation (4)) is completely different from the analytical solution, whereas the numerical solution obtained by using the CONDOR approach is in excellent agreement with it.

Next, the far-field scattered potential is analyzed. Figures 8–10 depict the directivity patterns for the scattering of an impinging plane wave, comparing the analytical solutions with the numerical ones, for $ka = 1$, $ka = 3$, and $ka = 5$,

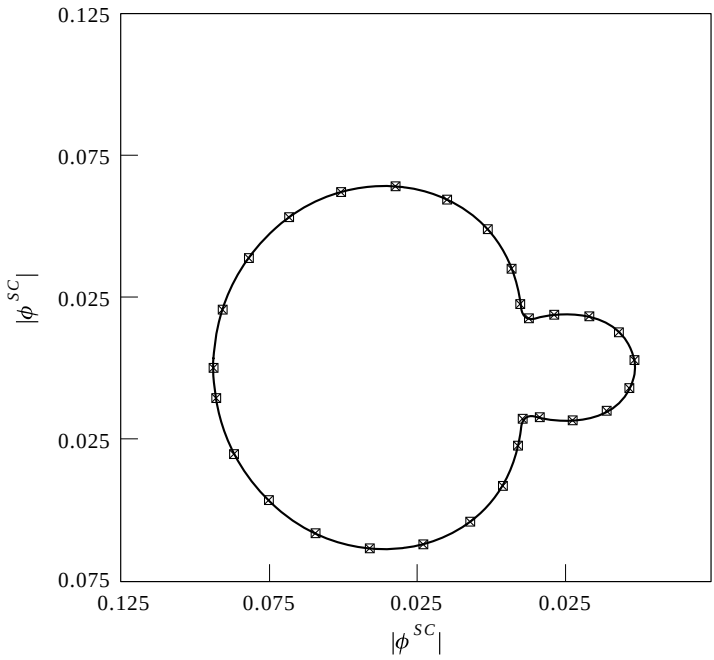

Figure 6. Angular dependence of potential scattered by a rigid sphere impinged by a unit-amplitude plane wave with $ka = 1$, at a distance $d = 5a$. ——, Analytical solution; □ – – – □, BEM equation (4) with $N = 48$; × — — ×, present formulation with $N = 48$.

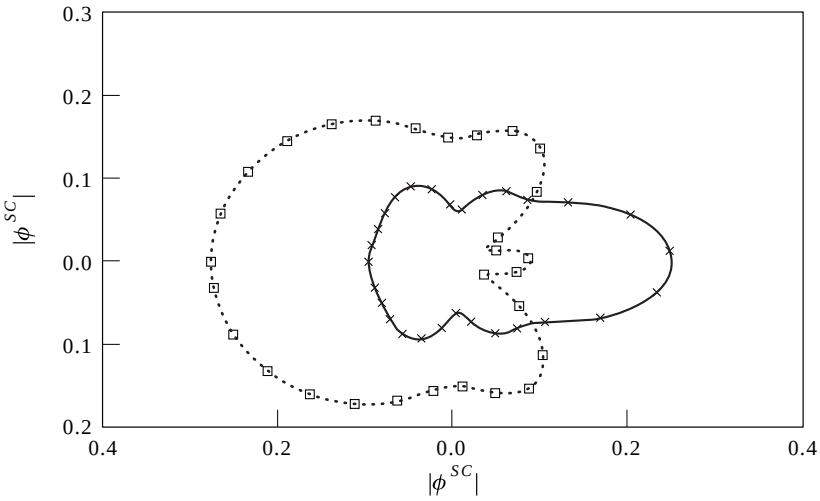

Figure 7. Angular dependence of potential scattered by a rigid sphere impinged by a unit-amplitude plane wave with $ka = \pi$, at a distance $d = 5a$. ——, Analytical solution; □ – – – □, BEM equation (4) with $N = 48$; × — — ×, present formulation with $N = 48$.

respectively. The numerical solutions have been evaluated with $N = 48$, and in all of the cases presented they are in excellent agreement with the analytical ones.

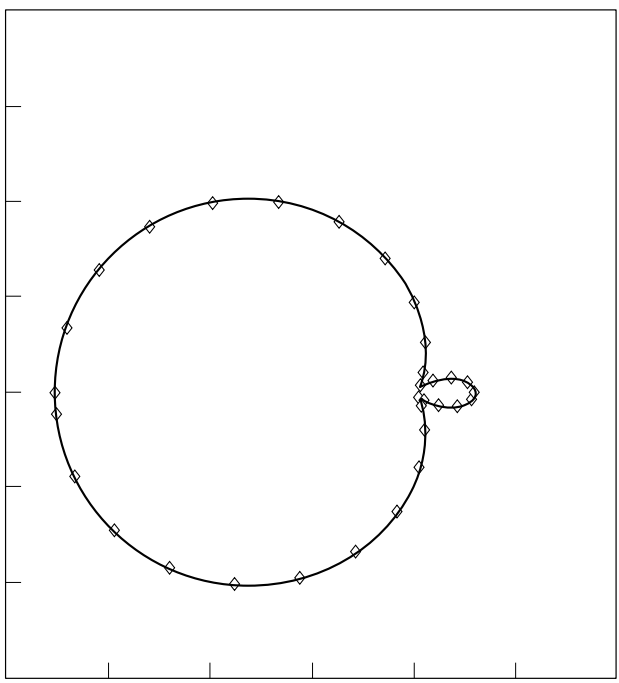

Figure 8. Directivity patterns for the scattering of a plane wave by a rigid sphere, when $ka = 1$. ——, Analytical solution: ◇ – – – ◇, present formulation with $N = 48$.

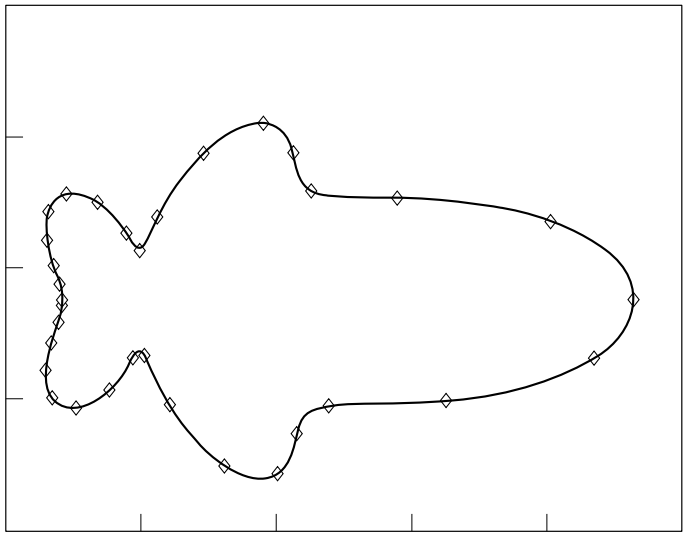

Figure 9. Directivity patterns for the scattering of a plane wave by a rigid sphere, when $ka = 3$. ——, Analytical solution: ◇———◇, present formulation with $N = 48$.

Next, consider the case of a high-frequency far-field scattered potential, for an impinging plane wave, with $ka = 30$. Figure 11 shows the analytical result, the numerical results for $N = 24$ and $N = 36$, and the converged numerical solution obtained by extrapolation (see Appendix C). In this case, due to the short wavelength, only the extrapolated solution is in agreement with the analytical one, whereas the solutions evaluated with $N = 24$ and $N = 36$ differ from it, since they do not capture perfectly the steep spatial variations of potential on the body surface (note that for $N = 24$ one has $\Delta s = 0{\cdot}625\lambda$, whereas for $N = 36$ one has $\Delta s = 0{\cdot}416\lambda$). A zoom of Figure 11 is presented in Figure 12, which depicts the same comparison as in Figure 11, but only for the region defined by $90° \leqslant \psi \leqslant 100°$ (where the polar angle, ψ, is such that $\psi = 0°$ along the direction

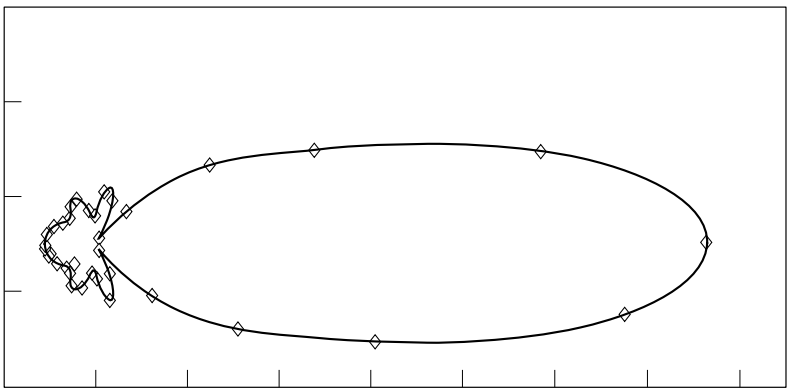

Figure 10. Directivity patterns for the scattering of a plane wave by a rigid sphere, when $ka = 5$. ——, Analytical solution: ◇———◇, present formulation with $N = 48$.

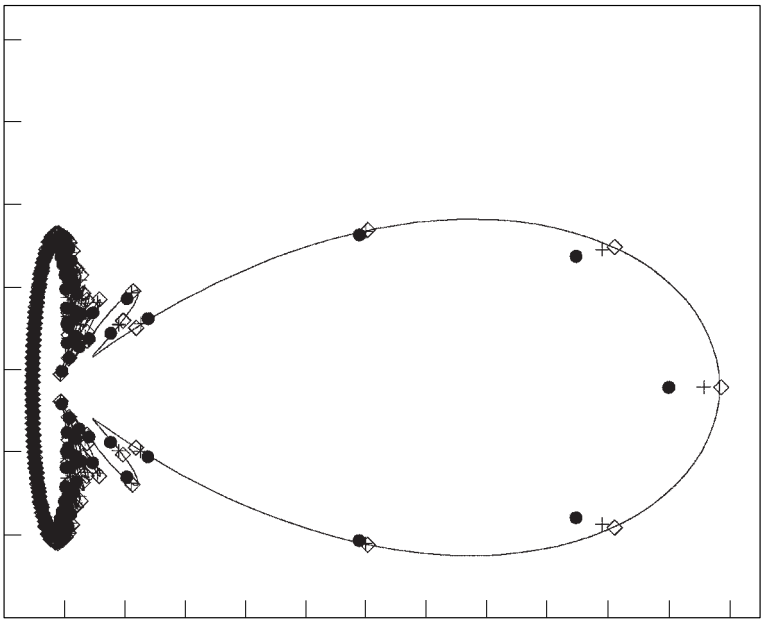

Figure 11. Directivity patterns for the scattering of a plane wave by a rigid sphere, when $ka = 30$. ——, Analytical solution; ●, present formulation with $N = 24$; +, present formulation with $N = 36$; ◇, extrapolated solution.

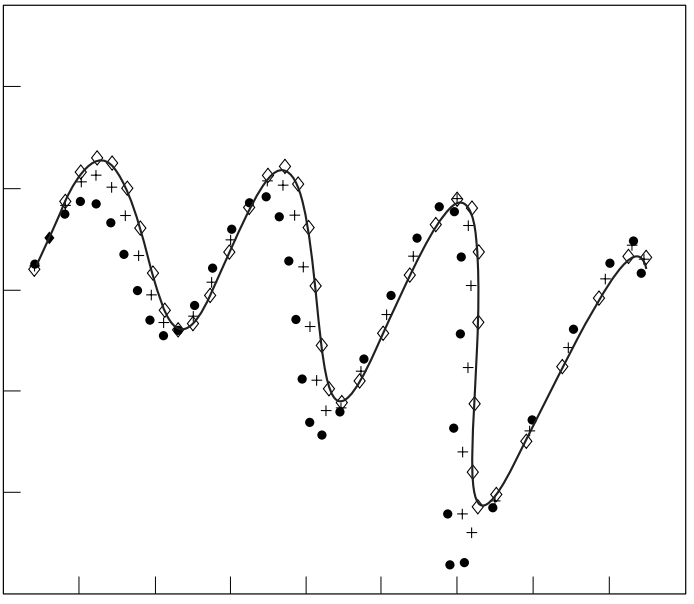

Figure 12. Directivity patterns for the scattering of a plane wave by a rigid sphere, when $ka = 30$, in the region defined by the polar angle, ψ, such that $90° \leqslant \psi \leqslant 100°$. ——, Analytical solution; ●, present formulation with $N = 24$; +, present formulation with $N = 36$; ◇, extrapolated solution.

from which the plane wave impinges the sphere). From this figure it is apparent that the extrapolated solution is still in excellent agreement with the analytical one (see Appendix C).

Note that, as expected, for the problem examined in this subsection the numerical solution has a third-order rate of convergence for low-frequency impinging waves. However, such rate of convergence has been obtained also in the more taxing problem of high-frequency impinging waves, as shown in Appendix C.

4.3. SCATTERING BY AN ELASTIC SPHERICAL SHELL

For the analysis of scattering by an elastic spherical shell impinged by a unit-amplitude plane wave, a shell of aluminium with thickness $\tau = 3$ mm, density $\varrho = 2700$ kg/m^3, Young's modulus $E = 72$ GPa, and Poisson's coefficient $\nu = 0{\cdot}3$ has been considered. The elastic motion of the spherical shell has been evaluated by applying the Lagrange equations of motion, where the Lagrangian variables are the coefficients in the expansion in terms of the modes of vibration of the shell (given in reference [21]; note that for a plane impinging wave, the elastic displacement of the spherical shell is axisymmetric).

First, consider the case of an impinging plane wave with $ka = 11{\cdot}15$, which corresponds to the first natural frequency of the elastic shell considered. The polar plot of the induced elastic displacement is illustrated in Figure 13 and shows a good agreement between the present numerical results and the analytical solution (all the numerical results presented in this subsection have been obtained by using the first 11 axisymmetric modes of vibration for the shell displacement, since with the addition of further modes the solution produces no significant changes). The potential scattered by the elastic sphere as a function of the polar angle is plotted in Figures 14 and 15 for distances from the center of the sphere $d/a = 3$ and $d/a = 5$, respectively. In both cases it is shown that, as the grid resolution used in the numerical computation increases, the numerical results get closer and closer to the analytical results.

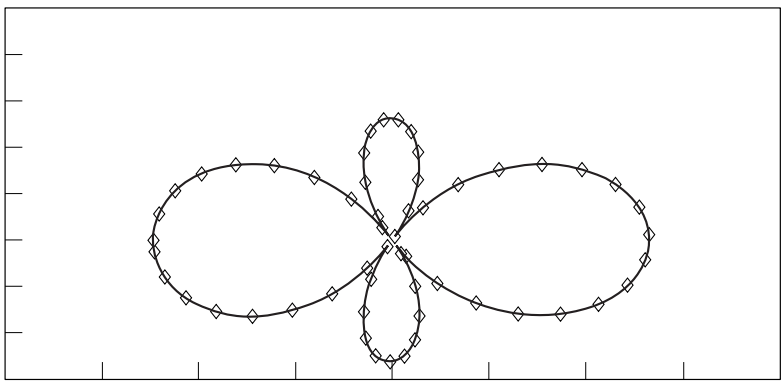

Figure 13. Polar plot of the displacement induced on an elastic spherical shell by a unit-amplitude impinging plane wave with $ka = 11{\cdot}15$. ——, Analytical solution; ◇– – –◇, present formulation with $N = 48$.

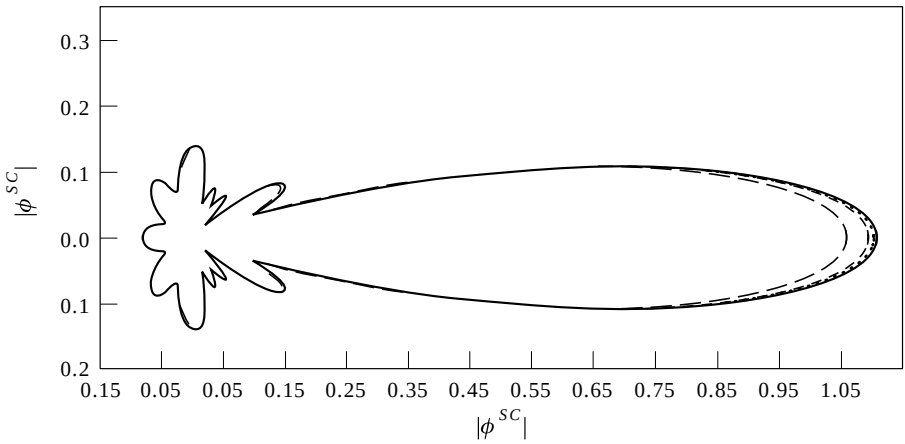

Figure 14. Angular dependence of potential scattered by an elastic spherical shell impinged by a unit-amplitude plane wave with $ka = 11{\cdot}15$, at a distance $d = 3a$. ——, Analytical solution; — — —, present formulation with $N = 24$; — — —, present formulation with $N = 36$; ----, present formulation with $N = 48$.

Then, consider the capabilities of the method at higher frequencies. Figure 16 shows the elastic displacement of the sphere at the point of the sphere first impinged by the plane wave, as a function of the wave number. The comparison between the analytical solution and our numerical results with $N = 24$ indicates a good agreement. The corresponding scattered potential (evaluated at a point placed along the direction from which the plane wave impinges the sphere, and at a distance $d = 5a$ from the center of it) is illustrated in Figure 17. In this figure, the analytical solution is compared with the present numerical results for $N = 24$ and $N = 48$. For very high values of the wave number, the accuracy of

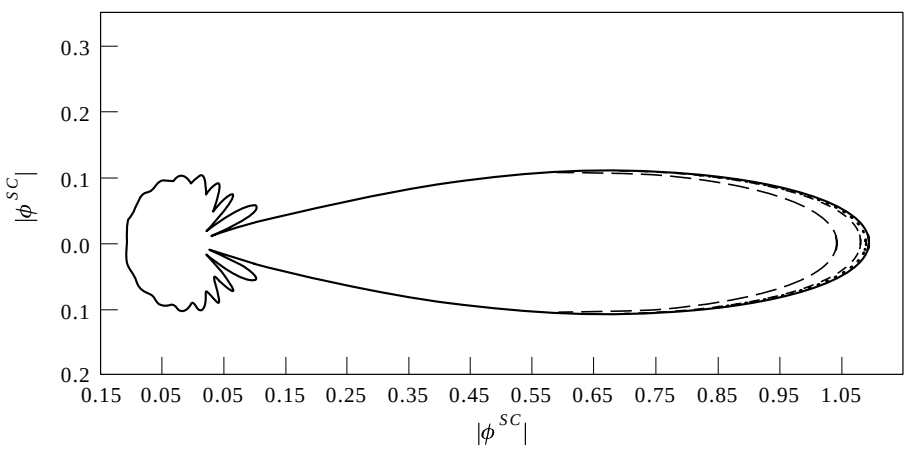

Figure 15. Angular dependence of potential scattered by an elastic spherical shell impinged by a unit-amplitude plane wave with $ka = 11{\cdot}15$, at a distance $d = 5a$. ——, Analytical solution; — — —, present formulation with $N = 24$; — — —, present formulation with $N = 36$; ----, present formulation with $N = 48$.

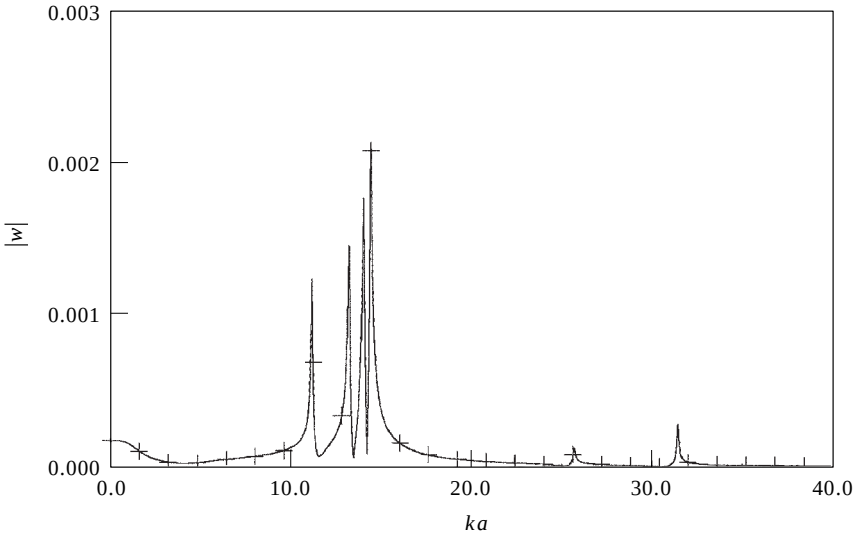

Figure 16. Amplitude of displacement on an elastic spherical shell impinged by a unit-amplitude plane wave as a function of the wave number. ——, Analytical solution; + – – – +, present formulation with $N = 24$.

the numerical result with $N = 24$ has a dramatic decrease, whereas the solution with $N = 48$ maintains a satisfactory agreement with the analytical one, for $ka < 30$.

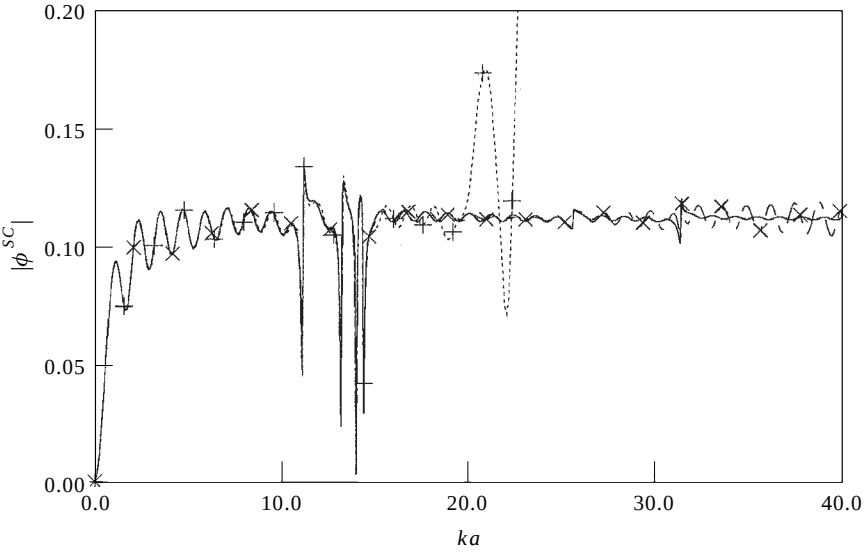

Figure 17. Amplitude of potential scattered by an elastic spherical shell impinged by a unit-amplitude plane wave as a function of the wave number, for $d = 5a$. ——, Analytical solution; + – – – +, present formulation with $N = 24$; × — — ×, present formulation with $n = 48$.

Finally, a convergence analysis of the numerical solution has been accomplished also for the case of elastic shells. In Appendix C it is shown that, as obtained for rigid shells, the convergence rate of the numerical solution is of third-order and perfectly matches the analytical solution.

5. CONCLUDING REMARKS

A novel third-order boundary element method for the prediction of sound scattered by rigid or elastic shells impinged by plane waves has been presented. The occurrence of spurious frequencies, introduced by the boundary element methodology has been overcome by the CONDOR approach. The hypersingular kernel appearing in the resulting boundary integral equation has been regularized by introducing an integral equivalence between doublet layers and vortex layers for the Helmholtz equation.

From the analysis of the numerical results obtained, the following conclusions may be taken: (1) both in the case of a pulsating sphere and in the case of wave scattering by a rigid sphere, the application of the CONDOR approach efficiently eliminates the spurious frequencies and yields potential-field solutions in excellent agreement with the analytical ones; (2) the sound scattered by spherical rigid and elastic shells is predicted with excellent accuracy, both for low-frequency and high-frequency impinging plane waves; (3) the convergence rate of the numerical solution has been shown to be of third order, for all of the problems examined here (pulsating sphere, rigid/elastic spherical shell scattering, low-frequency and high-frequency impinging waves).

Therefore, the methodology presented in this work seems to be an efficient tool for the problem of sound scattering. However, the application to irregular scattering surfaces and to cases with very-high-frequency impinging waves needs additional work on the formulation presented.

REFERENCES

1. D. COLTON and R. KRESS 1983 *Integral Equation Methods in Scattering Theory*. New York: Wiley.
2. H. A. SCHENCK 1968 *Journal of Acoustical Society of America* **44**, 41–58. Improved integral formulation for acoustic radiation problems.
3. D. S. JONES 1974 *Quarterly Journal of Mechanics and Applied Mathematics* **27**, 129–142. Integral equations for the exterior acoustic problem.
4. F. URSELL 1978 *Mathematical Proceedings of Cambridge Philosophical Society* **84**, 545–548. On the exterior problems of acoustics: II.
5. S. AMINI 1993 *Computational Mechanics* **13**, 2–11. Boundary integral solution of the exterior Helmholtz problem.
6. S. AMINI and S. M. KIRKUP 1995 *Journal of Computational Physics* **118**, 208–221. Solution of Helmholtz equation in the exterior domain by elementary boundary integral methods.
7. J. M. GALLMAN, M. K. MYERS and F. FARASSAT 1991 *American Institute of Aeronautics and Astronautics Journal* **29**, 2038–2046. Boundary integral approach to the scattering of nonplanar acoustic waves by rigid bodies.
8. G. C. GAUNAURD 1989 *Applied Mechanics Reviews* **42**, 143–192. Elastic and acoustic resonance wave scattering.

9. S. AMINI and P. J. HARRIS 1990 *Computational Methods in Applied Mechanics and Engineering* **84**, 59–75. A comparison between various boundary integral formulation of the exterior acoustic problem.
10. S. AMINI, P. J. HARRIS and D. T. WILTON 1992 in *Lecture Notes in Engineering* (C. A. Brebbia and S. A. Orszag, editors) Volume 77. New York/Berlin: Springer. Coupled boundary and finite element methods for the solution of the dynamic fluid-structure interaction.
11. A. J. BURTON and G. F. MILLER 1971 *Proceedings of Royal Society of London* **A323**, 201–210. The application of integral equation methods to the numerical solution of some exterior boundary-value problems.
12. W. L. MEYER, W. A. BELL, B. T. ZINN and M. P. STALLYBRASS 1978 *Journal of Sound and Vibration* **59**, 245–262. Boundary integral solutions of three-dimensional acoustic radiation problems.
13. T. TERAI 1980 *Journal of Sound and Vibration* **69**, 71–100. On calculation of sound fields around three-dimensional objects by integral equation methods.
14. C. C. CHIEN, H. RAJIYAH and S. N. ATLURI 1990 *Journal of Acoustical Society of America* **88**, 918–973. An effective method for solving the hypersingular integral equations in 3-D acoustics.
15. L. MORINO, M. GENNARETTI and G. CALCAGNO 1995 *Symposium of the International Association for Boundary Element Methods, Hawaii*. A third-order BEM for potential aerodynamics.
16. M. GENNARETTI, G. CALCAGNO, A. ZAMBONI and L. MORINO 1998 *The Aeronautical Journal* **102**, 211–219. A high-order boundary element formulation for potential incompressible aerodynamics.
17. R. KRESS 1985 *Quarterly Journal of Mechanics and Applied Mathematics* **38**, 323–341. Minimising the condition number of boundary integral operators in acoustic and electromagnetic scattering.
18. F. J. RIZZO and D. J. SHIPPY 1977 *International Journal for Numerical Methods in Engineering* **11**, 1753–1768. An advanced boundary integral equation method for three dimensional thermoelasticity.
19. P. M. MORSE and K. U. INGARD 1968 *Theoretical Acoustics*, New York: McGraw-Hill.
20. M. C. JUNGER 1951 *Journal of Acoustical Society of America* **24**, 366–373. Sound scattering by thin elastic shells.
21. W. E. BAKER 1961 *Journal of Acoustical Society of America* **33**, 1749–1758. Axisymmetric modes of vibration of thin spherical shell.
22. R. G. CAMPBELL 1973 *Foundations of Fluid Flow Theory*, Reading, MA: Addison-Wesley.
23. G. K. BATCHELOR 1967 *An Introduction to Fluid Dynamics*, Cambridge, England: Cambridge University Press.

APPENDIX A: REGULARIZATION OF HYPERSINGULAR INTEGRAL

In the numerical implementation of the method described in this work, a critical aspect is the evaluation of the second integral term in equation (6). Indeed, the kernel $\nabla'[\partial G(\mathbf{x}', \mathbf{y})/\partial n]$ becomes hypersingular when $\mathbf{x}'$ tends to $\mathbf{x} \in \mathcal{S}$ (see section 1 for a list of references dealing with this subject).

Here, in order to regularize the hypersingular kernel appearing in equation (6), the general integral formula discussed in Appendix B is used. Indeed, if in equation (21) one sets $g = G$, where $G = G(\mathbf{x}', \mathbf{y})$ is the fundamental solution for the Helmholtz equation (and hence $\nabla^2 G = -k^2 G$, for $\mathbf{x}' \neq \mathbf{y}$), and observes that $\nabla' G = -\nabla G$, one obtains the following integral relation

$$\nabla' \int_{\mathcal{S}} f \frac{\partial G}{\partial n} \, \mathrm{d}\mathcal{S}(\mathbf{y}) = -\nabla' \times \int_{\partial \mathcal{S}} G f \, \mathrm{d}\mathbf{y} + \nabla' \times \int_{\mathcal{S}} G(\mathbf{n} \times \nabla_t f) \, \mathrm{d}\mathcal{S}(\mathbf{y}) + k^2 \int_{\mathcal{S}} f G \mathbf{n} \, \mathrm{d}\mathcal{S}(\mathbf{y}), \quad (15)$$

where $\mathrm{d}\mathbf{y}$ is defined in Appendix B (equation (15) may be considered as the extension to the Helmholtz equation of the well-known incompressible-potential-flow equivalence between doublet-layer velocity field and vortex-layer velocity field, see equation (29)).

Observing that

$$\nabla' \times \int_{\mathcal{S}} G(\mathbf{n} \times \nabla_t f) \, \mathrm{d}\mathcal{S}(\mathbf{y}) = \int_{\mathcal{S}} \nabla' G \times (\mathbf{n} \times \nabla_t f) \, \mathrm{d}\mathcal{S}(\mathbf{y}), \quad (16)$$

and using the vector relationship $\mathbf{a} \times (\mathbf{b} \times \mathbf{c}) = \mathbf{b}(\mathbf{a} \cdot \mathbf{c}) - \mathbf{c}(\mathbf{a} \cdot \mathbf{b})$, one obtains

$$\nabla' \times \int_{\mathcal{S}} G(\mathbf{n} \times \nabla_t f) \, \mathrm{d}\mathcal{S}(\mathbf{y}) = \int_{\mathcal{S}} \frac{\partial G}{\partial n} \nabla_t f \, \mathrm{d}\mathcal{S}(\mathbf{y}) - \int_{\mathcal{S}} (\nabla_t G \cdot \nabla_t f) \mathbf{n} \, \mathrm{d}\mathcal{S}(\mathbf{y}). \quad (17)$$

The last term in equation (17) becomes Cauchy singular if $\mathbf{x}'$ tends to $\mathcal{S}$. However, using equation (26) and applying the divergence theorem for tensor fields, equation (27), one may write

$$\int_{\mathcal{S}} (\nabla_t G \cdot \nabla_t f) \mathbf{n} \, \mathrm{d}\mathcal{S}(\mathbf{y}) = \int_{\partial \mathcal{S}} G(\nabla_t f \cdot \mathbf{v}) \mathbf{n} \, \mathrm{d}\ell(\mathbf{y}) - \int_{\mathcal{S}} G \mathbf{n} \nabla_t^2 f \, \mathrm{d}\mathcal{S}(\mathbf{y}) - \int_{\mathcal{S}} G[\nabla_t \mathbf{n}] \nabla_t f \, \mathrm{d}\mathcal{S}(\mathbf{y}), \quad (18)$$

since $\nabla_t f \cdot \mathbf{n} = 0$. Next, combining equation (15) with equations (17) and (18), one obtains

$$\nabla' \int_{\mathcal{S}} f \frac{\partial G}{\partial n} \, \mathrm{d}\mathcal{S}(\mathbf{y}) = -\nabla' \times \int_{\partial \mathcal{S}} G f \, \mathrm{d}\mathbf{y} - \int_{\partial \mathcal{S}} G(\nabla_t f \cdot \mathbf{v}) \mathbf{n} \, \mathrm{d}\ell(\mathbf{y}) + \int_{\mathcal{S}} \frac{\partial G}{\partial n} \nabla_t f \, \mathrm{d}\mathcal{S}(\mathbf{y}) + \int_{\mathcal{S}} G \mathbf{n} \nabla_t^2 f \, \mathrm{d}\mathcal{S}(\mathbf{y}) + \int_{\mathcal{S}} G[\nabla_t \mathbf{n}] \nabla_t f \, \mathrm{d}\mathcal{S}(\mathbf{y}) + k^2 \int_{\mathcal{S}} f G \mathbf{n} \, \mathrm{d}\mathcal{S}(\mathbf{y}). \quad (19)$$

Finally, one can describe the regularization technique that has been used in this work. It consists of dividing the closed surface $\mathcal{S}$ in equation (6) into two portions: (1) an open surface $\mathcal{S}_*$ with the point $\mathbf{x}$ in its interior, and (2) its complement $\mathcal{S}_*^c = \mathcal{S} \backslash \mathcal{S}_*$. Over the surface $\mathcal{S}_*^c$ all the integral terms in equation (6) are regular, whereas over the surface $\mathcal{S}_*$ equation (19) is applied with $f = \varphi^S$. This yields the regularized form of equation (6), which has expression

$$\frac{\partial \varphi^S}{\partial n}(\mathbf{x}) = \lim_{\mathbf{x}' \to \mathbf{x}} \mathbf{n}_x(\mathbf{x}) \cdot \left\{ - \int_{\mathcal{S}} \frac{\partial \varphi^S}{\partial n} \nabla G \, \mathrm{d}\mathcal{S}(\mathbf{y}) + \int_{\mathcal{S}_*^c} \varphi^S \nabla \frac{\partial G}{\partial n} \, \mathrm{d}\mathcal{S}(\mathbf{y}) \right.$$
$$- \int_{\partial \mathcal{S}_*} \varphi^S \nabla G \times \mathrm{d}\mathbf{y} + \int_{\partial \mathcal{S}_*} G(\nabla_t \varphi^S \cdot \mathbf{v}) \mathbf{n} \, \mathrm{d}\ell(\mathbf{y}) - \int_{\mathcal{S}_*} \frac{\partial G}{\partial n} \nabla_t \varphi^S \, \mathrm{d}\mathcal{S}(\mathbf{y})$$
$$\left. - \int_{\mathcal{S}_*} G \mathbf{n} \nabla_t^2 \varphi^S \, \mathrm{d}\mathcal{S}(\mathbf{y}) - \int_{\mathcal{S}_*} G[\nabla_t \mathbf{n}] \nabla_t \varphi^S \, \mathrm{d}\mathcal{S}(\mathbf{y}) - k^2 \int_{\mathcal{S}_*} \varphi^S G \mathbf{n} \, \mathrm{d}\mathcal{S}(\mathbf{y}) \right\}, \tag{20}$$

where all integrals over the surface $\mathcal{S}_*$ are weakly singular.

APPENDIX B: AN INTEGRAL FORMULA

In this appendix the following integral formula is proved

$$\int_{\mathcal{S}} f [\nabla(\nabla g)] \mathbf{n} \, \mathrm{d}\mathcal{S} = - \int_{\partial \mathcal{S}} f \nabla g \times \, \mathrm{d}\mathbf{y} + \int_{\mathcal{S}} \nabla g \times (\mathbf{n} \times \nabla_t f) \, \mathrm{d}\mathcal{S} + \int_{\mathcal{S}} f \nabla^2 g \mathbf{n} \, \mathrm{d}\mathcal{S}, \tag{21}$$

where $\mathcal{S}$ is an arbitrary smooth open surface having $\mathbf{n}$ as unit normal, f and g are two differentiable scalar fields (f needs be defined only over $\mathcal{S}$), and $\nabla_t(\,) = \nabla(\,) - \mathbf{n}\partial(\,)/\partial n$ denotes the tangential gradient operator over the surface $\mathcal{S}$, applied to a scalar field (note that the co-ordinate direction n normal to $\mathcal{S}$ has been chosen such that $\partial \mathbf{n}/\partial n = 0$). Furthermore, $\mathrm{d}\mathbf{y} = \mathbf{n} \times \mathbf{v} \, \mathrm{d}\ell$, where $\mathbf{v}$ denotes the outward unit vector orthogonal to $\partial \mathcal{S}$ and lying in the plane tangent to $\mathcal{S}$, whereas $\mathrm{d}\ell$ denotes the infinitesimal portion of the line $\partial \mathcal{S}$.

In order to accomplish this, consider the integral term

$$\mathcal{I} = \int_{\mathcal{S}} \nabla g \times (\mathbf{n} \times \nabla_t f) \, \mathrm{d}\mathcal{S}, \tag{22}$$

which, using the vector relationship $\mathbf{a} \times (\mathbf{b} \times \mathbf{c}) = \mathbf{b}(\mathbf{a} \cdot \mathbf{c}) - \mathbf{c}(\mathbf{a} \cdot \mathbf{b})$, becomes

$$\mathcal{I} = \int_{\mathcal{S}} (\nabla_t g \cdot \nabla_t f) \mathbf{n} \, \mathrm{d}\mathcal{S} - \int_{\mathcal{S}} \frac{\partial g}{\partial n} \nabla_t f \, \mathrm{d}\mathcal{S}. \tag{23}$$

Then, applying the following integral formula for a differentiable scalar field h (gradient theorem for a smooth surface)

$$\int_{\mathcal{S}} \nabla_t h \, \mathrm{d}\mathcal{S} = \int_{\partial \mathcal{S}} h \mathbf{v} \, \mathrm{d}\ell + \int_{\mathcal{S}} \mathcal{H} h \mathbf{n} \, \mathrm{d}\mathcal{S}, \tag{24}$$

the second integral in equation (23) may be recast as

$$\int_{\mathcal{S}} \frac{\partial g}{\partial n} \nabla_t f \, \mathrm{d}\mathcal{S} = \int_{\partial \mathcal{S}} f \frac{\partial g}{\partial n} \mathbf{v} \, \mathrm{d}\ell + \int_{\mathcal{S}} \mathcal{H} f \frac{\partial g}{\partial n} \mathbf{n} \, \mathrm{d}\mathcal{S} - \int_{\mathcal{S}} f \nabla_t \left(\frac{\partial g}{\partial n} \right) \mathrm{d}\mathcal{S}, \tag{25}$$

where $\mathcal{H} = \nabla \cdot \mathbf{n}$ denotes the mean curvature of the surface $\mathcal{S}$.

Next, introduce the following tangential differential operators on any surface with unit normal $\mathbf{n}$: (1) for a differentiable tensor field $\mathbf{T}$, $\nabla_t \cdot \mathbf{T} = \nabla \cdot \mathbf{T} - \partial(\mathbf{Tn})/\partial n$, (2) for a differentiable vector field $\mathbf{v}$, $\nabla_t \mathbf{v} = \nabla \mathbf{v} - (\partial \mathbf{v}/\partial n) \otimes \mathbf{n}$, and (3) for a differentiable scalar field h, the tangential Laplacian $\nabla_t^2 h = \nabla^2 h - \partial^2 h/\partial n^2 - \mathcal{H}\partial h/\partial n$. From these definitions, it is easy to verify that,

$$(\nabla_t g \cdot \nabla_t f)\mathbf{n} = \nabla_t \cdot (f\mathbf{n} \otimes \nabla_t g) - f\mathbf{n}\nabla_t^2 g - f[\nabla_t \mathbf{n}]\nabla_t g. \tag{26}$$

Then, using the following integral formula for a differentiable tensor field, $\mathbf{T}$ (divergence theorem for a smooth surface)

$$\int_{\mathcal{S}} \nabla_t \cdot \mathbf{T}\, \mathrm{d}\mathcal{S} = \int_{\partial\mathcal{S}} \mathbf{Tv}\, \mathrm{d}\ell + \int_{\mathcal{S}} \mathcal{H}\mathbf{Tn}\, \mathrm{d}\mathcal{S}, \tag{27}$$

the first term in equation (23) may be recast as

$$\int_{\mathcal{S}} (\nabla_t g \cdot \nabla_t f)\mathbf{n}\, \mathrm{d}\mathcal{S} = \int_{\partial\mathcal{S}} f\mathbf{n}\nabla_t g \cdot \mathbf{v}\, \mathrm{d}\ell - \int_{\mathcal{S}} f\mathbf{n}\nabla_t^2 g\, \mathrm{d}\mathcal{S} - \int_{\mathcal{S}} f[\nabla_t \mathbf{n}]\nabla_t g\, \mathrm{d}\mathcal{S}. \tag{28}$$

Finally, combining equation (22) and equation (23) with equations (25) and (28), observing that $\nabla(\partial g/\partial n) = [\nabla \mathbf{n}]\nabla g + [\nabla(\nabla g)]\mathbf{n}$, and recalling that $\partial \mathbf{n}/\partial n = 0$, one obtains the integral equivalence given in equation (21).

Note that, for incompressible potential flow, if in equation (21) one sets $g = G$, where $G = G(\mathbf{x}', \mathbf{y})$ is the fundamental solution for the Laplace equation (and hence $\nabla^2 G = 0$, for $\mathbf{x}' \neq \mathbf{y}$), and observes that $\nabla' G = -\nabla G$, one obtains the well-known equivalence between the velocity field induced by a doublet layer with intensity f and that induced by a vortex layer with vorticity $\boldsymbol{\gamma} = \mathbf{n} \times \nabla_t f$ (see also references [22, 23]):

$$\nabla' \int_{\mathcal{S}} f \frac{\partial G}{\partial n}\, \mathrm{d}\mathcal{S}(\mathbf{y}) = -\nabla' \times \int_{\partial\mathcal{S}} Gf\, \mathrm{d}\mathbf{y} + \nabla' \times \int_{\mathcal{S}} G\boldsymbol{\gamma}\, \mathrm{d}\mathcal{S}(\mathbf{y}). \tag{29}$$

APPENDIX C: CONVERGENCE ANALYSIS

In this appendix the convergence rate of the method presented in this work is analyzed. Three cases have been examined: (1) the convergence of the solution around the pulsating sphere considered in section 4.1, (2) the convergence of potential scattered by rigid and elastic spherical shells impinged by a unit-amplitude low-frequency plane wave (problems discussed in sections 4.2 and 4.3), and (3) the convergence of potential scattered by a rigid shell impinged by a unit-amplitude high-frequency plane wave (problem discussed in section 4.2).

Figure A1 shows the convergence history of the solution (expressed in terms of potential) around a pulsating sphere with $ka = \pi$ (first spurious resonance frequency of the exterior Neumann problem). It demonstrates that the rate of convergence of the solution is of the third order (linear in $1/N^3$) and that the (linear in $1/N^3$) extrapolation for $N \to \infty$ yields the analytical solution (as stated

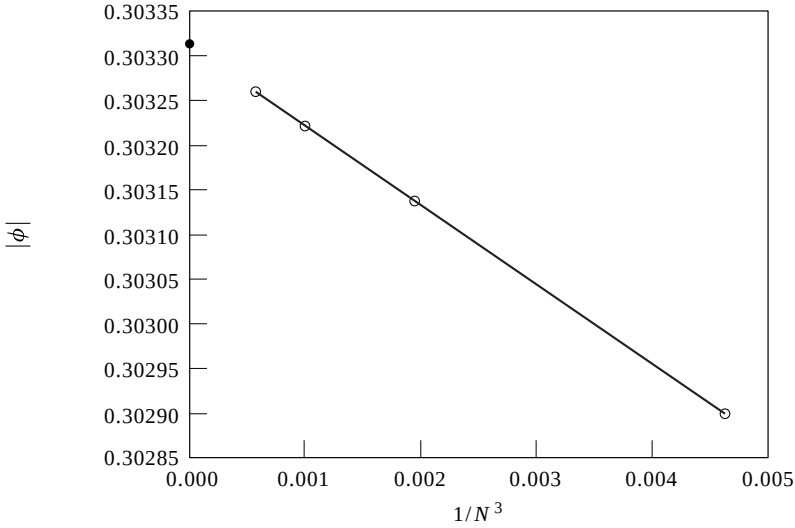

Figure A1. Convergence analysis for the potential on the surface of a pulsating sphere with pulsation wave number $ka = \pi$. ●, Analytical solution; ○, present formulation.

in section 4.1, N represents the number of elements along the meridians of the spherical surface, and half of the number of elements along the parallels).

A similar behavior has also been observed in the convergence analysis of the potential scattered by rigid and elastic spherical shells impinged by a plane wave. Indeed, in Figure A2 the potential scattered at a point placed along the direction from which the plane wave impinges the sphere, is plotted as a function of the

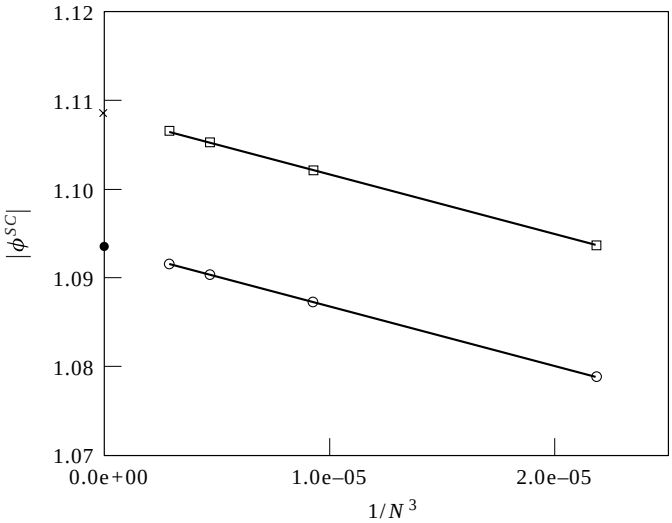

Figure A2. Convergence analysis for the potential scattered both by a rigid and by an elastic spherical shell impinged by a unit-amplitude plane wave with $ka = 11{\cdot}15$, for $d = 5a$. ●, Analytical solution for rigid shell; ×, analytical solution for elastic shell; ○, present formulation for rigid shell; □, present formulation for elastic shell.

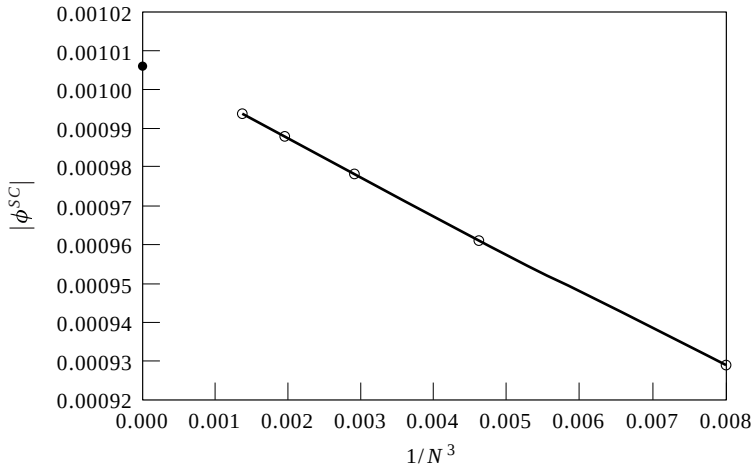

Figure A3. Convergence analysis for the potential scattered by a rigid sphere impinged by a unit-amplitude plane wave with $ka = 30$. ●, Analytical solution; ○, present formulation.

inverse of the third power of N (in this case $ka = 11{\cdot}15$ and $d = 5a$). As shown in the figure, also in the case of wave scattering by both rigid and elastic shells, the rates of convergence are of third order and the extrapolations (linear in $1/N^3$) for $N \to \infty$ yield the analytical solutions.

Finally, consider the case of far-field scattered potential for a plane wave with $ka = 30$, impinging a rigid sphere. In particular, the convergence rate of the solution is analyzed at one of the points included in Figure 12, where the polar plot shows a highly wavy behavior of the scattered potential. Figure A3 shows that, even in this critical region, the convergence rate is of third order and the (linear in $1/N^3$) extrapolation for $n \to \infty$ yields the analytical solution.